

CHAPTER 2

THEORETICAL APPROACH



2.1 Moment-Curvature Relationship

Theoretical moment-curvature curves for reinforced concrete sections with flexure and axial load can be derived from the basic assumptions that plane sections before bending remain plane after bending and the stress-strain curves for concrete and steel are known. The curvatures associated with a range of bending moments and axial loads may be determined using these assumptions and from the requirements of strain compatibility and equilibrium of forces.

Cross-sections of concrete girders are often composed of three types of material: prestressed steel, non-prestressed reinforcement and concrete which may exist in more than one type in one cross-section. Concrete exhibits the properties of creep and shrinkage, and in addition prestressed steel loses part of its tension due to relaxation. Thus, the components forming one section tend to have different strains. However, because of the bond, the difference in strain is restrained. Thus, the stresses in concrete and the two types of reinforcement change with time as creep, shrinkage and relaxation develop (Ghali and Favre, 1994). The assumptions for the girder analysis are:

1. The cross-sections considered are assumed to have one axis of symmetry and to be subjected to a bending and an axial force caused by prestressing or by other loading.
2. A perfect bond is assumed between concrete and steel; thus, at any fiber the strains in concrete and steel are equal. The slip that usually occurs at the extremities of the member is ignored.
3. Plane cross-sections are assumed to remain plane after deformation. No cracking is assumed in the analysis procedure.
4. With unbonded post-tensioning, the last assumption is not justified.

However, in most practical calculations the incompatibility in strain, which may develop after prestress transfer, between the strain in an unbonded tendon and the adjacent concrete is generally ignored.

In this part, the stress, strain and deformations of a member for the elongations or end rotation are not restrained by the supports or by continuity with other members. Creep, shrinkage and relaxation of steel change the distribution of stress and strain in the section but do not change the reactions and the induced stress resultants (values of the axial force or bending moment acting on the section).

Creep and shrinkage of concrete and relaxation of prestressed steel result in prestress loss and thus in time-dependent change of the internal forces (the resultant of stresses) on the concrete cross-section. Generally, in a prestressed section, non-prestressed reinforcement is also present. The time effects of creep, shrinkage and relaxation usually produce a reduction of tension in the prestressed steel and of compression in the concrete and an increase of compression in the non-prestressed steel.

At the time of prestressing, or at a later date, external loads are often introduced, as for example the self-weight. The internal forces due to such loading and the time of their application are assumed to be known. The initial prestressing is assumed to be known but the changes in the stress in the prestressed and non-prestressed steels and the concrete are determined by the analysis.

2.1.1 Strain Compatibility

Figure 2.1(a) is the cross-section of a member composed of different materials and having an axis of symmetry. Assume that the cross-section is subjected to a force N normal to the section situated at any point on the symmetry axis. Such a force is statically equivalent to a system composed of a normal force N at a reference point O and a bending moment M . The equations most commonly used in calculations of stress, strain and curvature at the cross-section are generally based on the assumption that O is the centroid of the transformed section.

When considering the effects of creep, the analysis of the same cross-section but different elasticity moduli for concrete and superposed with the stresses from several analyses will be done. Changing the value of E_c will result in a change of the centroid of the transformed section. To avoid this difficulty, the equations below for the strain, curvature and the stress distribution of a cross-section without requiring that the reference point O be the centroid of the cross-section will be derived. Thus, O is an arbitrarily chosen reference point on the axis of symmetry.

The strain distribution is assumed to be linear as shown in Fig. 2.1(b), in other works, a plane cross-section is assumed to remain plane after deformation. At any fiber, at a distance y from the reference point O , the strain is:

$$\varepsilon = \varepsilon_0 + \psi y \quad (2.1)$$

where ε_0 is the strain at the reference point and ψ is the curvature. The distance y is positive when the point considered is below the reference point.

When the fiber considered is in the i th part of the composite section, the stress at the fiber is

$$\sigma = E_i (\varepsilon_0 + \psi y) \quad (2.2)$$

Integration of the stress over the area of the cross-section and taking the moment about an axis through O , gives

$$N = \int \sigma dA \quad (2.3)$$

$$M = \int \sigma y dA \quad (2.4)$$

The integral is to be performed for all parts of the cross-section.

Substitution of Eq.(2.2) into Eqs.(2.3-2.4) gives

$$N = \varepsilon_0 \sum_{i=1}^m E_i \int dA + \psi \sum_{i=1}^m E_i \int y dA \quad (2.5)$$

$$M = \varepsilon_0 \sum_{i=1}^m E_i \int y dA + \psi \sum_{i=1}^m E_i \int y^2 dA \quad (2.6)$$

Thus summations in Eqs.(2.5-2.6) are to be performed from $i=1$ to m where m is the number of parts in the cross-section. Eqs.(2.5-2.6) may be rewritten

$$N = E_{ref} (A\varepsilon_0 + B\psi) \quad (2.7)$$

$$M = E_{ref} (B\varepsilon_0 + I\psi) \quad (2.8)$$

where A , B and I are the transformed cross-section area and its first and second moment about an axis through O . E_{ref} is modulus for the reference material among different materials in one section.

For a composite section, A , B and I are derived by summing up the contribution of the parts

$$A = \sum_{i=1}^m \left(\frac{E_i}{E_{ref}} A_i \right) \quad (2.9)$$

$$B = \sum_{i=1}^m \left(\frac{E_i}{E_{ref}} B_i \right) \quad (2.10)$$

$$I = \sum_{i=1}^m \left(\frac{E_i}{E_{ref}} I_i \right) \quad (2.11)$$

where A_i , B_i and I_i are respectively the area of the i th part and its first and second moment about an axis through O. A reinforcement layer may be treated as one part.

Eqs.(2.7-2.8) may be rewritten in the matrix form

$$\begin{bmatrix} N \\ M \end{bmatrix} = E_{ref} \begin{bmatrix} A & B \\ B & I \end{bmatrix} \begin{bmatrix} \varepsilon_0 \\ \psi \end{bmatrix} \quad (2.12)$$

This equation may be used to find N and M when ε_0 and ψ are known; or when N and M are known the equation may be solved for the axial strain and curvature:

$$\begin{bmatrix} \varepsilon_0 \\ \psi \end{bmatrix} = \frac{1}{E_{ref}(AI - B^2)} \begin{bmatrix} I & -B \\ -B & A \end{bmatrix} \begin{bmatrix} N \\ M \end{bmatrix} \quad (2.13)$$

2.1.2 Temperature Effect

In a statically determinate frame, a uniform or linearly varying temperature over the depth of the cross-section of a member produces no stresses. When the temperature variation is non-linear, stresses are produced because each fiber being attached to adjacent fibers is not free to acquire the full expansion due to temperature. The stresses produced in this way in an individual cross-section must be self-equilibrating; in other words the temperature stress in a statically determinate structure corresponds to no change in the stress resultants. The self-equilibrating stresses caused by non-linear temperature variation over the cross-sections of statically determinate frames are sometimes referred to as the eigen-stresses. If the structure is statically indeterminate, the elongation and/or the rotations of the joints of the members are restrained or prevented, resulting in a statically indeterminate set of reactions which are also self-equilibrating, but these will produce statically indeterminate internal forces and corresponding stresses.

The hypothetical strain that would occur at any fiber if it were free is:

$$\varepsilon_f = \alpha_f T \quad (2.14)$$

where $T = T(y)$, the temperature rise at any fiber at a distance y below a reference point O and $\alpha_t =$ coefficient of thermal expansion. The daily climatic changes introduce nonlinear temperature distributions in concrete structures (Fig. 2.2). These temperature variations over the depth can be approximately represented by a fourth-order polynomial interpolation (Thepchatri, 1975 and Priestley, 1978).

If this strain is artificially prevented, the stress in the restrained condition will be:

$$\sigma_{restrained} = -E\varepsilon_f \quad (2.15)$$

The resultant of this stress may be represented by an axial force ΔN at a reference point O and a bending moment ΔM given by

$$\Delta N = \int \sigma_{restrained} dA = - \int E\varepsilon_f dA \quad (2.16)$$

$$\Delta M = \int \sigma_{restrained} y dA = - \int E\varepsilon_f y dA \quad (2.17)$$

The artificial restraint is now released by the application of a force $-\Delta N$ at O and a bending moment $-\Delta M$; the resulting axial strain and curvature are obtained by:

$$\begin{bmatrix} \Delta\varepsilon_0 \\ \Delta\psi \end{bmatrix} = \frac{1}{E(AI - B^2)} \begin{bmatrix} I & -B \\ -B & A \end{bmatrix} \begin{bmatrix} -\Delta N \\ -\Delta M \end{bmatrix} \quad (2.18)$$

$$\Delta\sigma = E(\Delta\varepsilon_0 + (\Delta\psi)y) \quad (2.19)$$

The actual stress due to temperature is the sum of $\sigma_{restrained}$ and $\Delta\sigma$ thus:

$$\sigma = E(-\varepsilon_f + \Delta\varepsilon_0 + (\Delta\psi)y) \quad (2.20)$$

2.1.3 Time-Dependent Effect

Figure 2.3 shows the analysis of time-dependent stress and strain in a composite section.

2.1.3.1 Instantaneous Stress and Strain at Age t_0

The combination with the prestressing forces into an equivalent normal force at O and a moment is:

$$\begin{bmatrix} N \\ M \end{bmatrix}_{equivalent} = \begin{bmatrix} N - \sum P_i \\ M - \sum P_i y_{psi} \end{bmatrix} \quad (2.21)$$

The instantaneous axial strain and curvature immediately after prestressing are given by:

$$\begin{bmatrix} \varepsilon_0(t_0) \\ \psi(t_0) \end{bmatrix} = \frac{1}{E_{ref}(AI - B^2)} \begin{bmatrix} I & -B \\ -B & A \end{bmatrix} \begin{bmatrix} N \\ M \end{bmatrix}_{equivalent} \quad (2.22)$$

The instantaneous strain and stress in concrete at any fiber are:

$$\varepsilon_c(t_0) = \varepsilon_0(t_0) + \psi(t_0)y \quad (2.23)$$

$$\sigma_c(t_0) = [E_c(t_0)]_i [\varepsilon_0(t_0) + \psi(t_0)y] \quad (2.24)$$

The instantaneous stress in the non-prestressed steel is:

$$\sigma_{ns}(t_0) = E_{ns} [\varepsilon_0(t_0) + \psi(t_0)y] \quad (2.25)$$

In the case of pretensioning, the stress in the prestressed steel immediately after transfer is:

$$\sigma_{ps}(t_0) = (\sigma_{ps})_{initial} + E_{ps} [\varepsilon_0(t_0) + \psi(t_0)y] \quad (2.26)$$

The second term in this equation represents the instantaneous change in stress (generally a loss of tension due to shortening of concrete). Thus the instantaneous prestress change (loss) in pretensioned tendon at the time of transfer is:

$$(\Delta\sigma_{ps})_{inst} = E_{ps} [\varepsilon_0(t_0) + \psi(t_0)y] \quad (2.27)$$

With post-tensioning, compatibility of strain in the tendon does not take place at this stage and thus no instantaneous loss occurs.

2.1.3.2 Changes in Stress and Strain during the Period t_0 to t

In this step of the analysis we deal with a cross-section for which the initial stress and strain are known. Creep, shrinkage and relaxation of steel result in stress redistribution between the various materials involved. The analysis gives the stress changes in each material occurring during a specified period of time.

The change in strain during the period t_0 to t is defined by the increments $\Delta\varepsilon_0$ and $\Delta\psi$ in the axial strain and curvature. The change of strain due to creep and shrinkage of concrete and relaxation of prestressed steel is first artificially restrained by application of an axial force ΔN at O and a bending moment ΔM . Subsequently, these restraining forces are removed by the application of equal and opposite forces on the composite section, resulting in the following changes in axial strain and in curvature:

$$\begin{bmatrix} \Delta \varepsilon_0 \\ \Delta \psi \end{bmatrix} = \frac{1}{\bar{E}_c (\bar{AI} - \bar{B}^2)} \begin{bmatrix} \bar{I} & -\bar{B} \\ -\bar{B} & \bar{A} \end{bmatrix} \begin{bmatrix} -\Delta N \\ -\Delta M \end{bmatrix} \quad (2.28)$$

The restraining forces are calculated as a sum of three terms:

$$\begin{bmatrix} \Delta N \\ \Delta M \end{bmatrix} = \begin{bmatrix} \Delta N \\ \Delta M \end{bmatrix}_{creep} + \begin{bmatrix} \Delta N \\ \Delta M \end{bmatrix}_{shrinkage} + \begin{bmatrix} \Delta N \\ \Delta M \end{bmatrix}_{relaxation} \quad (2.29)$$

If creep were free to occur, the axial strain and curvature would increase during the period t_0 to t by the amounts $\varphi(t, t_0) \varepsilon(t_0)$ and $\varphi(t, t_0) \psi(t_0)$. The forces necessary to prevent these deformations may be determined by:

$$\begin{bmatrix} \Delta N \\ \Delta M \end{bmatrix}_{creep} = -\sum_{i=1}^m \left\{ \bar{E}_c \varphi \begin{bmatrix} A_c & B_c \\ B_c & I_c \end{bmatrix} \begin{bmatrix} \varepsilon_0(t_0) \\ \psi(t_0) \end{bmatrix} \right\}_i \quad (2.30)$$

The forces required to prevent shrinkage are:

$$\begin{bmatrix} \Delta N \\ \Delta M \end{bmatrix}_{shrinkage} = -\sum_{i=1}^m \left\{ \bar{E}_c \varepsilon_{cs} \begin{bmatrix} A_c \\ B_c \end{bmatrix} \right\}_i \quad (2.31)$$

The forces necessary to prevent the strain due to relaxation of prestressed steel are:

$$\begin{bmatrix} \Delta N \\ \Delta M \end{bmatrix}_{relaxation} = \sum \begin{bmatrix} A_{ps} \Delta \bar{\sigma}_{pr} \\ A_{ps} y_{ps} \Delta \bar{\sigma}_{pr} \end{bmatrix}_i \quad (2.32)$$

The stress in concrete required to prevent creep and shrinkage at any fiber is

$$\sigma_{restrained} = -\bar{E}_c(t, t_0) [\varphi(t, t_0) \varepsilon_c(t_0) + \varepsilon_{cs}] \quad (2.33)$$

2.1.4 End Movements

From the analysis in the previous section, the results of axial strain and curvature in each section through the girder's length can be determined and can be changed to end movements of highway girders by principle of virtual work. The axial deformation can occur due to ambient temperature, prestress force, creep and shrinkage. The camber can occur due to prestress force, creep and temperature gradient. The deflection can occur due to external loads such as dead weight and live loads, as well as differential shrinkage between girder and deck.

2.1.4.1 Short-term Deflection

Fully prestressed concrete members are uncracked under service loads and are assumed linear elastic. Their instantaneous deflections can be determined using general principles of mechanics. Typical formulas are derived for simply supported beams with constant sectional properties. Commonly used expressions for calculating deflection are shown in Table 2.1 for various types of external loading and various profiles of a prestressing force assumed constant. Because superposition is valid in computing deflections for uncracked members, many combinations are practically covered in Table 2.1. The deflection (positive downward, negative upward) expressed as a function of the curvatures has the following general form:

$$\Delta_{v,mid} = \frac{\psi_c L^2}{8} - (\psi_c - \psi_e)(\gamma) \quad (2.34)$$

where ψ_c is mid-span curvature

ψ_e is end curvature

γ is multiplier for deflection

If the two end curvatures are not equal, use an average value of the two curvatures of ψ_e .

In addition, the equation for an approximate calculation from axial strain (ε) to axial deformation (Δ_H) is shown:

$$\Delta_H = \frac{\varepsilon_{ave} L}{2} \quad (2.35)$$

where ε_{ave} is average axial strain along girder length, L .

2.1.4.2 Long-term Deflection

If the load is sustained, such as in the case of dead loads, the deflection increases with time, mainly because of the effects of creep and shrinkage of the concrete and relaxation of prestressing steel. The additional long-term deflection increases with time. With time, the ratio of stress to total strain decreases due to the creep strain and the change of the properties of concrete with the progress of its hydration. These effects can be simulated by using an equivalent modulus. Due to the gradual development of the strains due to creep and shrinkage, the time-dependent forces developed by creep and shrinkage in the steel and in the concrete also develop gradually. The response of the concrete to gradually changing stress is best calculated

by Bazant's age-adjusted effective modulus formula, \overline{E}_c (Bazant, 1972). Creep and shrinkage reduce the intrinsic relaxation of prestressing steel. Based on a step-by-step numerical procedure and the relaxation-time function developed by Magura (1964), a chart has been developed which gives the relaxation reduction coefficient, χ_r , that can be taken equal to 0.8.

Creep, shrinkage and relaxation of prestressing steel change the distribution of stress and strain in the section but do not change the reactions and the induced stress resultants (values of the axial force or bending moment acting on the section).

There are various methods for computing long-term deformations in prestressed concrete members.

1. The simplified prediction method suggested the multipliers of instantaneous deflection to estimate the additional long-term deflection. This method suggested a range of the multipliers based on the experience of designers. It was later developed by Leslie (1977) under some assumptions and used as a design tool in PCI Design Handbook (1988) as shown in Table 2.2.
2. The incremental time steps method was suggested by ACI Committee 435. This method may include the following steps: dividing the span into several segments, dividing the design life of the structure into several time intervals, selecting a time interval, and integrating or summing up the computed curvature along the beams.
3. The proposed pressure-line method proposed by Antoine (1983) to predict long-term deflections combines the theory behind the time-steps method with some simplified observations. It has the advantage of being relatively simple and sufficiently accurate for a number of practical cases, yet manageable in terms of computational effort.

2.2 Cracking and Tension Stiffening

Cracking in reinforced concrete structures is unavoidable due to the low tensile strength of the concrete. To control the crack width at the member surface of structures including link slabs, designers may use the guidelines prescribed in various

building codes. Inspection of crack width prediction procedures proposed by various investigators indicates that each formula contains a different set of variables and there is no general agreement among various investigators on the relative significance of different variables affecting the crack width. Cracking in a reinforced concrete member also causes a significant increase in deflection. This is a result of the reduction of bending stiffness at cracked sections. However, at sections between successive cracks, some tensile stress is retained in the concrete around steel bars due to the action of bond, contributing to the bending stiffness of the member. This is called the tension-stiffening effect. The tension-stiffening effect is incorporated in a semi-empirical manner by using the effective moment of inertia method.

2.2.1 Crack Width and Crack Spacing

The development of crack spacing and crack width prediction formulae is usually based on calculated concrete stress distributions within the tensile zone of a member. Different investigators have used various simplified analytical procedures to determine the concrete tensile stress. While some analytical investigations are coupled with experimental works to verify the prediction formulas, there are some investigations totally based on test results. It is agreed by all investigators that crack width increases with the steel stress at the crack section. It is also agreed that the concrete strength has no significant effect on the crack width; only the equation proposed by Venkateswarlu & Gesund (1972) includes the concrete strength in terms of the modular ratio. Depending on the conclusions drawn by different investigators, variables such as bar diameter, reinforcement ratio and concrete cover are embedded in prediction formulas differently. An increase in the bar diameter and concrete cover, as well as a decrease in the reinforcement ratio increase the crack width, if all other variables are kept constant.

The formation of the first crack affects the concrete and steel stresses for a certain distance, S_0 , on either side of the crack. This distance is governed by bond characteristics of reinforcement and the increase in steel stress due to the formation of the crack. The concrete stress at the tension face of the member increases gradually from zero at the crack to the maximum at the end of the distance S_0 . Consequently, the spacing of these cracks or primary cracks is predicted to be regular spacing S_0 in a

varying moment region, and any value between S_0 and $2S_0$ in a constant moment region.

Figure 2.4 shows a beam AB subjected to two equal point loads at C and D such that the bending moment along the length CD is constant. Line $A'C'D'B'$ represents the calculated tensile stress at the tension face of the beam, before the first flexural crack is developed. The line $A''B''$ indicates the modulus of rupture of the member that varies slightly above and below a mean value along the length of the member. Since the concrete stress at the tension face between C and D is constant, the first crack would occur at the point which has the lowest modulus of rupture between C and D . Once this crack is developed, the concrete stress at the tension face will be redistributed within a distance of S_0 on either side of the crack. The minimum primary crack spacing S_{pm} in a constant moment region can be expressed as

$$S_{pm} = S_0 \quad (2.36)$$

The second crack occurs at the point that has the next lowest modulus of rupture within the constant moment region, and beyond a distance S_0 away from the first crack. If two primary cracks are more than $2S_0$ apart, then intermediate cracks can be developed in between them. Therefore, the maximum primary crack spacing S_{px} in a constant moment region can be expressed as

$$S_{px} = 2S_0 \quad (2.37)$$

The locations of primary cracks in the constant moment region may vary randomly such that the spacing of adjacent primary cracks S_p is in between $2S_0$ and S_0 .

$$S_0 \leq S_p \leq 2S_0 \quad (2.38)$$

Figure 2.5 shows a beam AB subjected to a central point load. The calculated tensile stress at the tension face of the beam is shown by the line $A'C'B'$, which has the same shape as the bending moment diagram. $A''B''$ indicates the variation of the flexural strength along the beam. First crack will occur near the center of the beam where the tensile stress is highest. When the load is increased further tensile stresses will reach the modulus of rupture resulting in two new cracks equally distant from the first crack. Therefore, the primary cracks in a varying moment region are equally spaced at a distance S_0 .

$$S_p = S_0 \quad (2.39)$$

The maximum concrete tensile stress between successive cracks (primary cracks) in a constant moment region occurs at the mid section between the cracks,

while in a varying moment region its location is closer to the crack having the smaller moment. The magnitude of this maximum stress increases with the crack spacing as well as the load level on the beam. When the maximum concrete stress between adjacent cracks reaches the modulus of rupture, a secondary crack develops between the two primary cracks.

2.2.2 Short-Term Deflection

After the cracking, the bending stiffness along the length of the member varies which makes the calculation of deflections complicated. In a cracked beam, the bending stiffness is largest at sections within the uncracked region while it is smallest at cracked sections. At intermediate sections between adjacent cracks, the concrete around reinforcement retains some tensile force due to the action of the bond. These tensile forces cause a reduction in steel stress as well as a movement of the zero-strain plane towards the tension face. As a result, the bending stiffness at sections between adjacent cracks becomes larger than those at the adjacent cracked sections, contributing to an overall increase in the stiffness of the member. This effect is known as tension-stiffening. For an accurate assessment of deflection, the tension-stiffening effect needs to be incorporated in the calculation. The parameters affecting the tension-stiffening include a decrease or an increase of loading, the amount and distribution of reinforcement, the bar diameter, the bond and tensile strength of concrete, concrete cover and crack spacing. There are different procedures of incorporating the tension-stiffening effect in deflection calculation which are used at the effective moment of inertia, and used for the non-linear stress-strain relationship for tensile concrete.

2.2.2.1 Effective Moment of Inertia

In this method the short-term deflection is calculated using an average moment of inertia for the entire structure. Its value is taken, depending on the load intensity, in between the gross moment of inertia I_g for the uncracked section and the moment of inertia I_{cr} for a cracked section. Various formulas to calculate the effective moment of inertia I_e are shown below.

Branson (1963) proposed the model for effective moment of inertia of cracked reinforced concrete beams and one-way slabs subjected to a uniformly distributed load:

$$I_e = I_{cr} + (I_g - I_{cr}) \left(\frac{M_{cr}}{M_a} \right)^m \leq I_g : m = 3 \quad (2.40)$$

Al Zaid et al. (1991) suggested that the value of I_e calculated using Branson's formula may be increased by 20% for beams and one-way slabs subjected to central point loads.

Al Shaik & Al Zaid (1993) indicated that m in Branson's formula decreases with the amount of tensile reinforcement ratio ρ as shown below:

$$m = 3 - 0.8\rho \quad (2.41)$$

Grossman (1981) developed the following formula which eliminates the requirement of computing I_{cr} :

$$\frac{I_e}{I_g} = \left(\frac{M_{cr}}{M_a} \right)^2 \leq 1.0; \text{ if } \frac{M_a}{M_{cr}} \leq 1.6 \quad (2.42a)$$

$$\frac{I_e}{I_g} = 0.1K^* \left(\frac{M_a}{M_{cr}} \right) \geq 0.35K^*; \text{ if } \frac{M_a}{M_{cr}} > 1.6 \quad (2.42b)$$

$$K^* = \left(\frac{d/h}{0.9} \right) \left[\frac{\sqrt{2330/w_c}}{0.4 + (1.4M_a/M_u)(f_y/690)} \right] \quad (2.42c)$$

Rangan (1982) replaced the mid span moment M_a by the service moment M_s , which was calculated as the moment of resistance when the steel stress is equal to 60% of the yield stress:

$$\frac{I_e}{bd^3} = 0.1599\sqrt{n\rho}; \text{ if } n\rho > 0.045 \quad (2.43a)$$

$$\frac{I_e}{bd^3} = 0.0019/n\rho; \text{ if } n\rho \leq 0.045 \quad (2.43b)$$

where M_a = maximum bending moment ($M_a > M_{cr}$)

M_{cr} = cracking moment of the member

w_c = unit weight of concrete (kg/m^3)

f_y = yield strength of steel (MPa)

2.2.2.2 Nonlinearity of Tensile Stress-strain Relationship

Another way of incorporating the tension-stiffening effect in deflection calculations is the use of the smeared crack approach, where the concrete tensile stress is averaged over representative lengths to span several cracks. In this method, the concrete tensile stress at a given section is calculated using a non-linear stress-strain relationship that allows the concrete to retain a certain amount of tensile stress beyond the cracking strain. The most commonly used non-linear stress-strain relationship is comprised of a curvilinear descending branch beyond the cracking strain of concrete, which is described below:

$$f_t = f_t' \left(\frac{\varepsilon}{\varepsilon'} \right); \text{ if } \left(\frac{\varepsilon}{\varepsilon'} \right) \leq 1 \quad (2.44a)$$

$$f_t = \frac{\beta f_t' \left(\frac{\varepsilon}{\varepsilon'} \right)}{\beta - 1 + \left(\frac{\varepsilon}{\varepsilon'} \right)^\beta}; \text{ if } \left(\frac{\varepsilon}{\varepsilon'} \right) > 1 \quad (2.44b)$$

where ε is concrete tensile strain

f_t is corresponding concrete stress

f_t' is tensile strength of concrete

β is parameter, which governs the rate of declining the tension stiffening effect with the increase of applied loading, depending on the sectional properties of the member (between 1.5 and 3.0)

In using the above constitutive relationship for calculating the concrete stress, a perfect bond between steel reinforcement and surrounding concrete is assumed. It must be noted however that the bond slip is not ignored in this method; the effect of bond slip is incorporated in the steepness of the descending branch of the stress-strain curve. For example, a steeper descending branch represents a member that loses most of the tension-stiffening effect for smaller slip values. This procedure is used in MASA finite element which will be mentioned in section 2.3.



2.3 Finite Element Method

2.3.1 MASA Program

In recent years a significant progress in modeling of concrete like materials for general stress-strain histories has been achieved. Presently available models for concrete can roughly be classified into two categories: (1) Macroscopic models, in which the material behavior is considered to be an average response of a rather complex microstructural stress transfer mechanism and (2) microscopic models, where the micromechanics of deformation is described by stress-strain relations on the micro level. No doubt, from the physical point of view microscopic models are more promising. However, they are computationally extremely demanding. Therefore, in practical application macroscopic models have to be used.

At the macro scale the model has to correctly describe microstructural phenomena such as cohesion, friction, aggregate interlock and interaction of microcracks. Cracking and damage phenomena can principally be modeled in two different ways: (1) the discrete crack model or (2) the smeared crack model. Traditionally, macroscopic models are formulated by total or incremental formulation between the σ_{ij} and ϵ_{ij} components of the stress and strain tensor, using the theory of tensorial invariants (Willam, 1974; Ortiz, 1985). In the framework of the theory there are various possible approaches for modelling of concrete, such as the theory of plasticity, the plastic-fracturing theory, continuum damage mechanics, endocronic theory and their combinations of various forms.

However, due to the complexity of concrete these models can not always realistically represent the behavior of concrete for general three-dimensional stress-strain histories. Therefore, to formulate a more general and relatively simple model significant effort has recently been made to further develop the microplane model for concrete (Bažant and Prat, 1988; Ožbolt and Bažant, 1992; Carol et al., 1992; Ožbolt et al., 1999). Some of the latest versions of the microplane model (Ožbolt et al., 1999) confirm that the model is able to realistically simulate concrete response for arbitrary loading histories.

The classical local continuum smeared fracture analysis of materials which exhibit softening (quasi-brittle materials) leads in the finite element analysis to the

results which are in general mesh dependent. As is well known, the reason for this is localization of damage and related energy consumption capacity which depends on the element size, i.e. if the finite element mesh is coarse the energy consumption capacity will be larger than if the mesh is fine. Consequently, the model response depends on the mesh size (Fig. 2.6). To ensure a mesh-independent result the total energy consumption capacity has to be independent of the element size, i.e. one has to regularize the problem by introducing the so-called localization limiter.

Currently two different approaches are in use. The first one is the relatively simple crack band method (Bažant and Oh, 1983) and the second group of approaches are the so-called higher order methods: Cosserat-continuum (de Borst, 1991), nonlocal continuum of integral type (Pijaudier-Cabot and Bažant, 1987; Ožbolt and Bažant, 1996) or nonlocal gradient type of continuum (de Borst, 1991). Compared to the crack band method the higher order procedures are rather complex, but more general. To obtain mesh-independent results one can alternatively use the discrete crack approach. However, the main drawback of this approach is the need for continuous re-meshing which is rather complex and time consuming. Moreover, some stress-strain histories (for instance compression) are difficult to model in a discrete sense. Therefore, the smeared crack approach is a more general approach, especially for practical engineering applications.

2.3.2 Microplane Material Model for Concrete

In the microplane model the material is characterized by a relation between the stress and strain components on planes of various orientations. These planes may be imagined to represent the damaged planes or weak planes in the microstructure, such as contact layers between aggregates in concrete. In the model the tensorial invariance restrictions need not be directly enforced. They are automatically satisfied by superimposing the responses from all microplanes in a suitable manner. The basic concept behind the microplane model was advanced in 1938 by Taylor. Later the model was extended by Bažant and co-workers for modeling of quasi-brittle materials which exhibit softening (Bažant and Prat, 1988; Ožbolt and Bažant, 1992; Carol et al., 1992; Ožbolt et al., 1999).

The advanced version of the microplane model for concrete was recently proposed by Ožbolt et al. (1999). It is based on the so-called relaxed kinematic

constraint concept. In the model the microplane is defined by its unit normal vector of components n_i (Fig. 2.7). Normal and shear stress and strain components ($\sigma_N, \sigma_{Tr}, \varepsilon_N, \varepsilon_{Tr}$) are considered on each plane. Microplane strains are assumed to be the projections of the macroscopic strain tensor ε_{ij} (kinematic constraint). Based on the virtual work approach, the macroscopic stress tensor is obtained as an integral over all possible, in advance defined, microplane orientations:

$$\sigma_{ij} = \frac{3}{2\pi} \int_{\Omega} \sigma_N n_i n_j d\Omega + \frac{3}{2} \int_{\Omega} \frac{\sigma_{Tr}}{2} (n_i \delta_{rj} + n_j \delta_{ri}) d\Omega \quad (2.45)$$

To realistically model concrete, the normal microplane stress and strain components have to be decomposed into volumetric and deviatoric parts ($\sigma_N = \sigma_V + \sigma_D, \varepsilon_N = \varepsilon_V + \varepsilon_D$), which leads to the following expression for the macroscopic stress tensor:

$$\sigma_{ij} = \sigma_V \delta_{ij} + \frac{3}{2\pi} \int_{\Omega} \sigma_D n_i n_j d\Omega + \frac{3}{2\pi} \int_{\Omega} \frac{\sigma_{Tr}}{2} (n_i \delta_{rj} + n_j \delta_{ri}) d\Omega \quad (2.46)$$

For each microplane component, the uniaxial stress-strain relations are assumed as:

$$\sigma_V = F_V(\varepsilon_{V,eff}); \quad \sigma_D = F_D(\varepsilon_{D,eff}); \quad \sigma_{Tr} = F_{Tr}(\varepsilon_{Tr,eff}) \quad (2.47)$$

From known macroscopic strain tensors, the microplane strains are calculated based on the kinematic constraint approach. However, in Eq. (2.47) only effective parts of these strains are used to calculate microplane stresses. Finally, the macroscopic stress tensor is obtained from Eq. (2.46). Integration over all microplane directions (21 directions) is performed numerically.

To model concrete cracking for any load history realistically, the effective microplane strains are used. They are calculated as:

$$\varepsilon_{m,eff} = \varepsilon_m \psi \quad (2.48)$$

where subscript m denotes corresponding microplane component (V, D, Tr) and ψ is so-called discontinuity function. This function accounts for discontinuity of the macroscopic strain field (cracking) on the individual microplanes. It relaxes the kinematic constraint which is in the case of localization of strains physically unrealistic. Consequently, in the smeared fracture type of the analysis the discontinuity function ψ enables localization of strains, not only for tensile fracture, but also for dominant compressive and shear type of failure.

The proposed model is implemented into the finite element code and a rather broad experience has been gained with it so far. Some of its qualities are:

1. Its conceptual simplicity, i.e. only a set of uniaxial stress-strain curves on the microplane need to be defined and the macroscopic model response comes automatically out as a result of the numerical integration over a number of microplanes
2. It covers the full three-dimensional range of applicability
3. It is relatively easy to account for initial anisotropy
4. The comparison between test data and the model response for different stress-strain histories shows good agreement
5. Implementation in the finite element code and a number of numerical studies that have been carried out indicated the capability of the model in realistic prediction of concrete behavior for different stress-strain histories.

2.3.3 Constitutive Law for Reinforcement

The constitutive law for steel is defined by uniaxial stress-strain law. Presently the three-linear stress-strain curve can be used. The curve is defined by four parameters: (1) Initial Young's modulus E_0 , (2) hardening modulus E_t , (3) yield stress f_y , (4) tensile (compressive) strength f_s .

2.3.4 Localization limiters

2.3.4.1 Crack Band Method

The main assumption of the crack band method is that damage (crack) is localized in a row of finite elements. To assure a constant and mesh independent energy consumption capacity of concrete (concrete fracture energy G_f) the constitutive law needs to be modified such that:

$$G_f = A_f h = \text{const.} \quad (2.49)$$

where A_f = area under the uniaxial compressive stress-strain curve and h = average element size (width of the crack band). Principally, the same relation is valid for

uniaxial compression with the assumption that the concrete compressive fracture energy G_c is a material constant:

$$G_c = A_{fc} h = \text{const.} \quad (2.50)$$

In which A_{fc} = area under the uniaxial compressive stress-strain curve. It is assumed that G_c is approximately 100 times larger than G_F ($G_c \approx 100G_F$). From Eqs. (2.49) and (2.50) it is obvious that the constitutive law for concrete need to be adopted to the element size.

Although the crack band method provides results which are independent of the element size, they can still depend on the form and orientation (alignment) of the finite element. This is especially true when the mesh is relatively coarse or the material is extremely brittle. To reduce this dependency and at the same time to keep the simplicity and relatively low computational costs of the crack band method a new so-called “Stress Relaxation Method” (Ožbolt, 1999) was developed and implemented into the code. The method is a combination of the standard crack band approach and the non-local approach of integral type. Due to the low computational costs and, compared to the standard crack band approach, reduced sensitivity to the shape of the mesh, the method is appropriate for practical applications.

2.3.4.2 Non-local Integral Approach

The non-local integral continuum approach offers a more general possibility to avoid spurious mesh dependency in the smeared fracture analysis of quasi-brittle materials. An effective form of the approach in which all variables that control the softening are non-local and all others are local (non-local strain approach of integral type) was proposed by Pijaudier-Cabot and Bažant (1987). The key parameter in this approach is the so-called characteristic length l . This length controls the size of the representative volume in which the local quantities are averaged (Bažant and Ožbolt, 1990).

In the non-local continuum concept the stress at a point depends not only on the strain at the same point but also on the strains in the domain V_R which is defined in advance. In general, the local variable that controls damage needs to be replaced by its non-local counterpart obtained by weighted averaging over a spatial neighborhood

of each point under the consideration. If $f(x)$ is the local variable which controls the material model response, then the corresponding non-local variable is defined as:

$$\bar{f}(x) = \frac{1}{V_R(x)} \int_V \alpha(x, s) f(s) dV(s) = \int_V \alpha'(x, s) f(s) dV(s) \quad (2.51)$$

The bar overscript denotes the averaging operator; $\alpha(x)$ = non-local weighting function; x and s are coordinate vectors of averaging and contributing points, respectively; V = volume of the entire structure and V_R = the representative volume calculated as:

$$V_R(x) = \int_V \alpha(x, s) dV(s), \quad \alpha'(x, s) = \frac{\alpha(x, s)}{V_R(x)} \quad (2.52)$$

The non-local weighting function is often taken as the Gauss distribution function:

$$\alpha(r) = \exp\left(-\frac{r^2}{2l^2}\right), \quad r = |s - x| \quad (2.53)$$

where l is the internal (characteristic) length of the non-local continuum. Another possible choice is the bell-shaped function:

$$\alpha(r) = \begin{cases} \left(1 - \frac{r^2}{R^2}\right), & 0 \leq r \leq R \\ 0 & R \leq r \end{cases} \quad (2.54)$$

where R (radius) is the parameter related but not equal to the characteristic length.

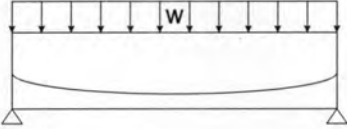
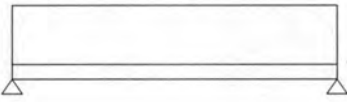
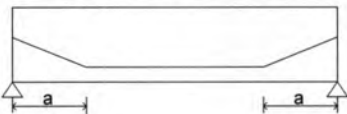
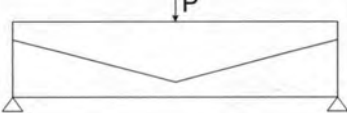
The variable which is to be averaged must be chosen such that the non-local solution exactly agrees with the local solution as long as the material behavior remains in the elastic range. Furthermore, for homogeneous stress-strain field the non-local solution must be identical with the local one. Principally, the choice of the variable which is to be averaged is rather arbitrary. However, practically the choice depends on the type of the constitutive law e.g. plasticity theory, damage theory, microplane model, etc.

It was first assumed that l is a material property related to the maximum aggregate size d_a ($l = 3d_a$). However, it turned out that the characteristic length generally depends not only on the composition of concrete. Namely, it has been found that the optimum value of l/d_a depends on the stress-strain state. This means that the characteristic length is not a material constant. Therefore, to improve the concept, a

new non-local approach of integral type which finds the physical background in the interaction of microcracks has been proposed by Bažant (1991) and implemented into a finite element code by Ožbolt and Bažant (1996).

In the FE-code MASA both above mentioned non-local approaches are implemented. Theoretically, they are more general than the relatively simple crack band approach. Using these procedures the results of the analysis are mesh-independent. However, according to the experience made in the last years there is still a number of problems which make the use of non-local approaches in practical applications for concrete and reinforced concrete structures difficult. The results are generally realistic only for relatively fine meshes. Consequently, the computational costs are often too high and the approach can not practically be used. This is especially true for three-dimensional simulations.

Table 2.1 Formula for end rotation of uncracked members

Curvature shape due to tendon profile or load	Midspan curvature, ψ_c	End curvature, ψ_e	Multiplier for deflection, γ	End rotation formula, θ
Parabolic profile or uniform loading 	$-\frac{P_{co}e_c}{E_{ci}I_g}$ $-\frac{wL^2}{8E_{ci}I_g}$	0	$\frac{L^2}{48}$	$\frac{\psi_c L}{3}$
Straight 	$-\frac{P_{co}e_c}{E_{ci}I_g}$	$-\frac{P_{co}e_e}{E_{ci}I_g}$	0	$\frac{\psi_c L}{2}$
Two point depressed tendon 	$-\frac{P_{co}e_c}{E_{ci}I_g}$	$-\frac{P_{co}e_e}{E_{ci}I_g}$	$\frac{a^2}{6}$	$\frac{\psi_c L}{2}$ $-(\psi_c - \psi_e)\frac{a}{2}$
One point depressed tendon 	$-\frac{P_{co}e_c}{E_{ci}I_g}$ $\frac{PL}{4}$	$-\frac{P_{co}e_e}{E_{ci}I_g}$ 0	$\frac{L^2}{24}$	$\frac{(\psi_c - \psi_e)L}{4}$

Note: P_{co} is prestress force in concrete, immediately after release

e_c is eccentricity of prestress force from centroid of section at center of span

e_e is eccentricity of prestress force from centroid of section at end of span

E_{ci} is modulus of elasticity of concrete at time of initial prestress

I_g is moment of inertia of gross section

Table 2.2 Multiplier for long-term deformations

Stage of Construction	Without Composite Topping	With Composite Topping
At erection		
Deflection (downward) component – apply to the elastic deflection due to the member weight at release of prestress	1.85	1.85
Camber (upward) component – apply to the elastic camber due to prestress at the time of release of prestress	1.80	1.80
Final		
Deflection (downward) component – apply to the elastic deflection due to the member weight at release of prestress	2.70	2.40
Camber (upward) component – apply to the elastic camber due to prestress at the time of release of prestress	2.45	2.20
Deflection (downward) – apply to elastic deflection due to superimposed dead load only	3.00	3.00
Deflection (downward) – apply to elastic deflection caused by the composite topping	-	2.30

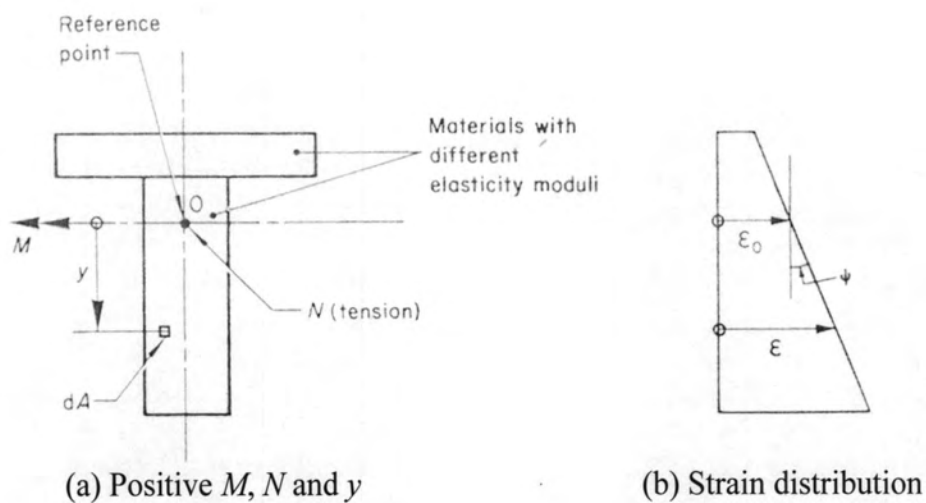


Fig. 2.1 Strain distribution in a composite cross-section

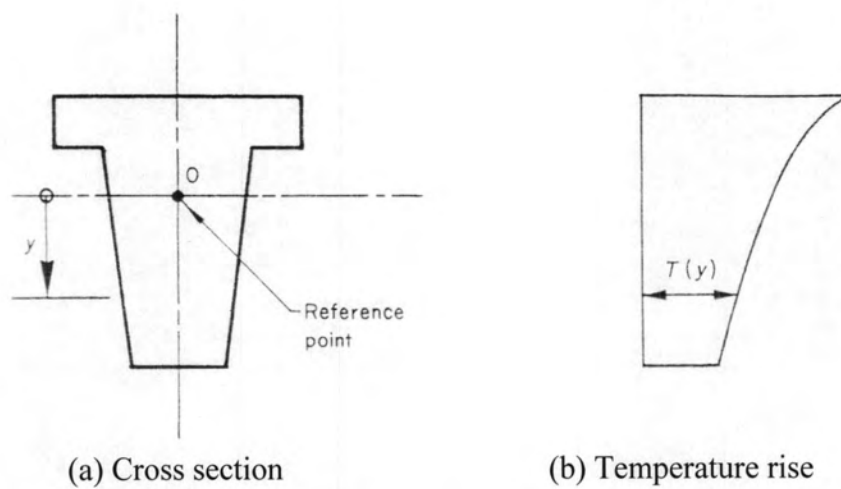


Fig. 2.2 Temperature rise which varies non-linearly over the depth

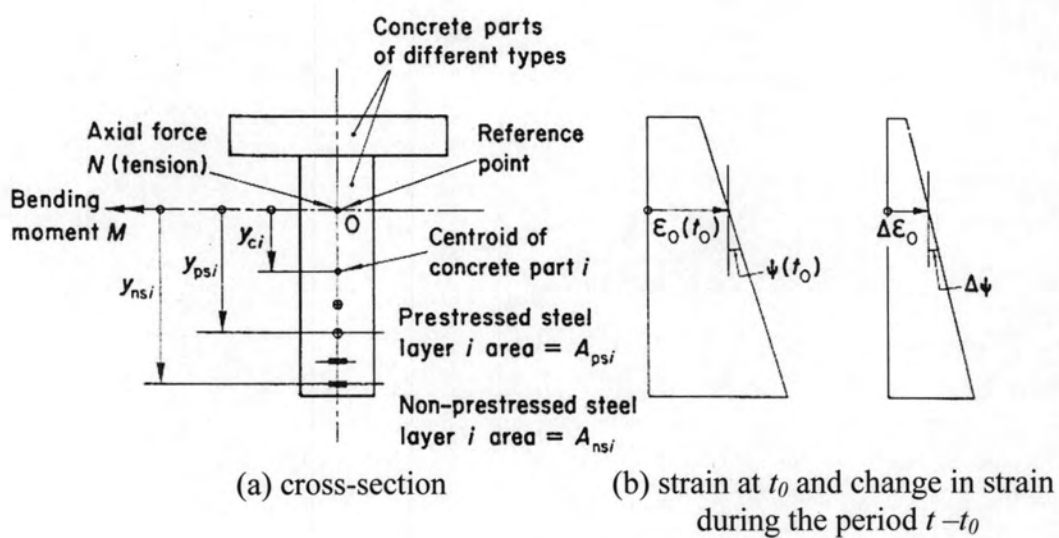


Fig. 2.3 Time-dependent strain distribution in a composite cross-section

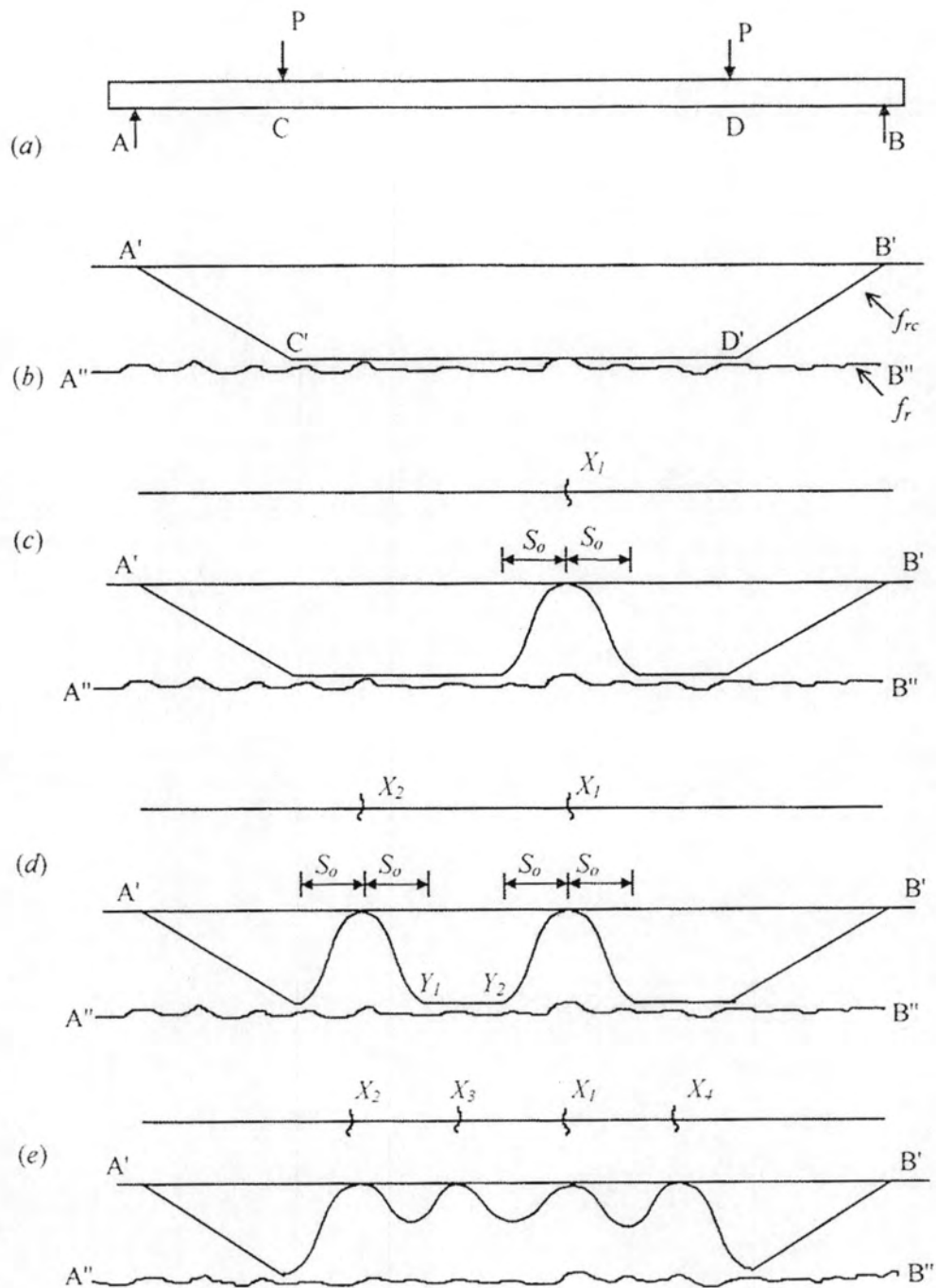


Fig. 2.4 Progressive development of primary cracks in a constant moment region

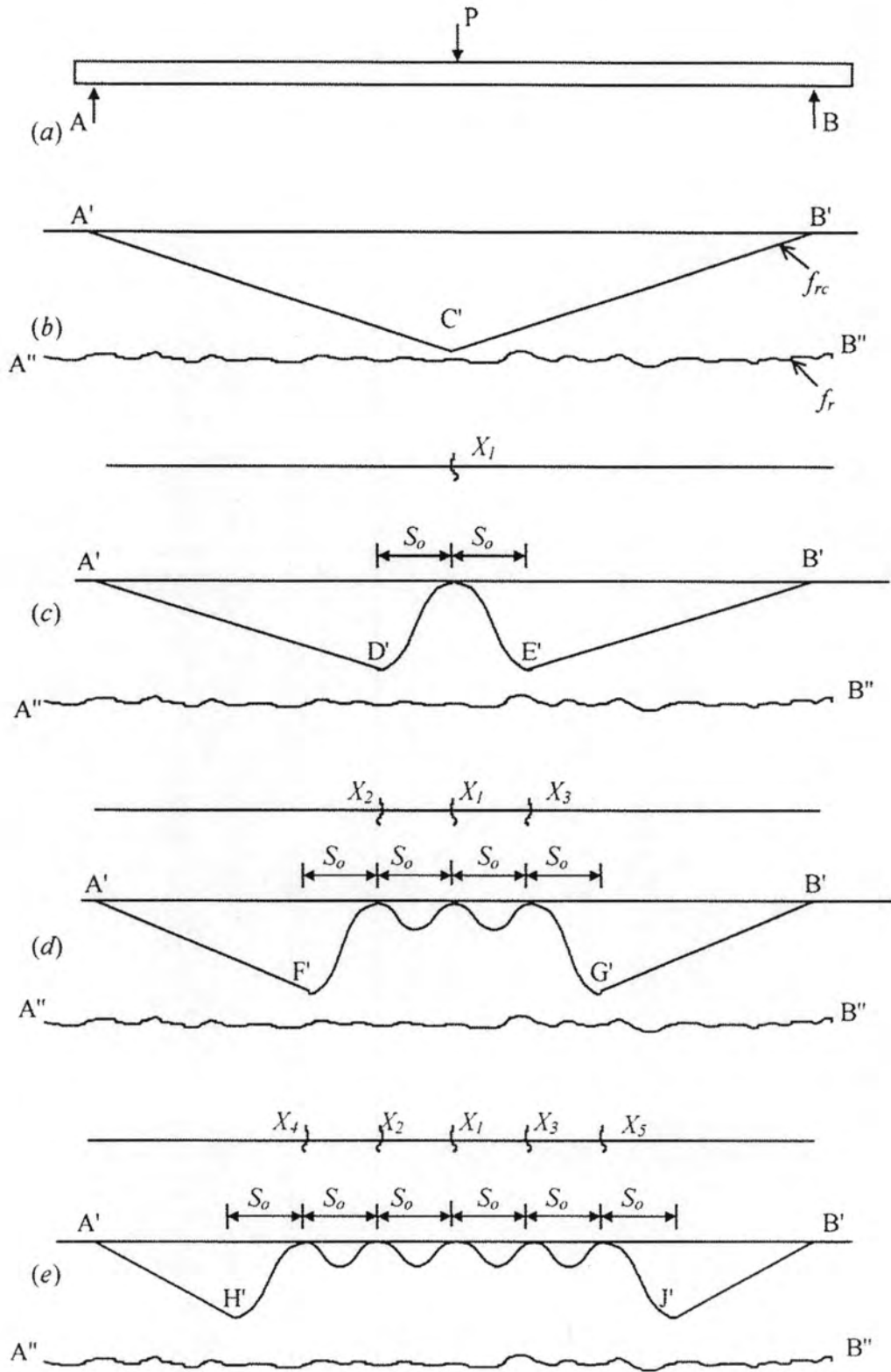


Fig. 2.5 Progressive development of primary cracks in a varying moment region

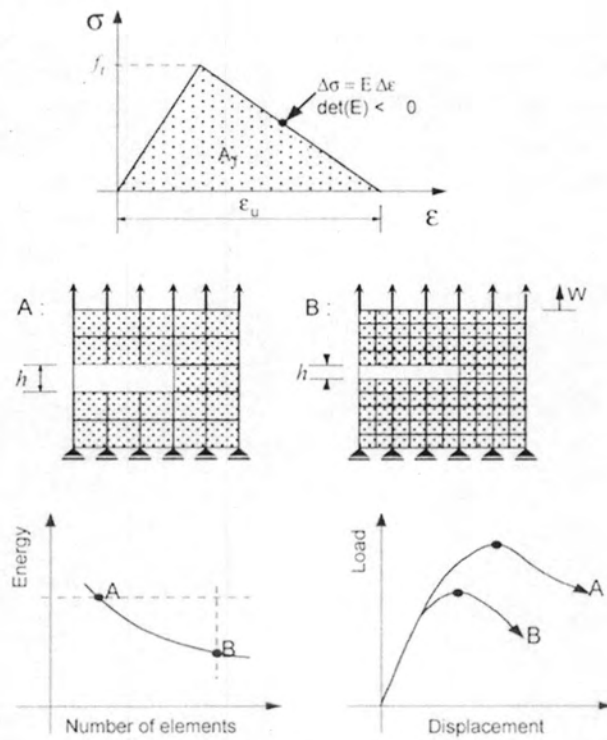
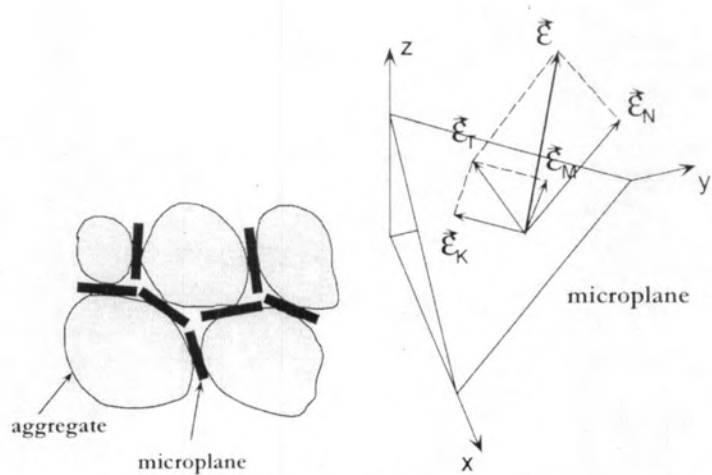
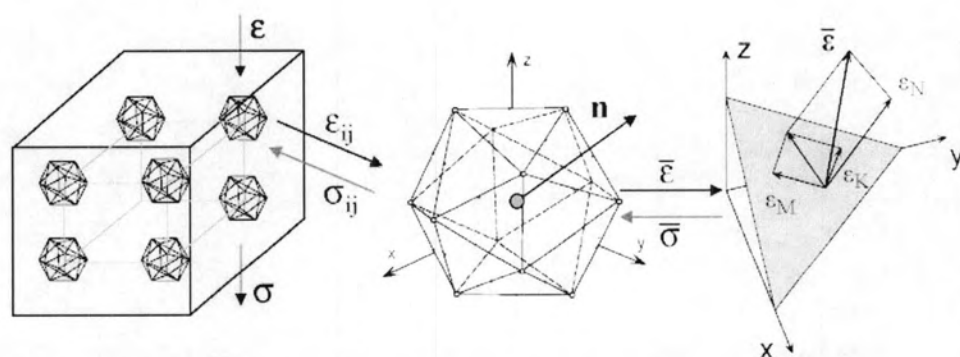


Fig. 2.6 Dependency of the local smeared crack FE analysis on the size of the finite elements



(a) Contact areas between the aggregate



(b) 3D solid FE (8 integration points), integration point and microplane

Fig. 2.7 Concept of the microplane model